Journal of Molecular Catalysis A: Chemical 307 (2009) 21–28

Contents lists available at ScienceDirect

Journal of Molecular Catalysis A: Chemical

journal homepage: www.elsevier.com/locate/molcata

Effects of steam addition on the spontaneous activation in Ni_3Al foil catalysts during methanol decomposition

Jun Hyuk Jang[a,b,*], Ya Xu[b], Dong Hyun Chun[c], Masahiko Demura[b], Dang Moon Wee[a], Toshiyuki Hirano[b]

[a] Department of Materials Science and Engineering, KAIST, 373-1, Guseong-dong, Yuseong-gu, Daejeon 305-701, Republic of Korea
[b] National Institute for Materials Science, 1-2-1 Sengen, Tsukuba, Ibaraki 305-0047, Japan
[c] Korea Institute of Energy Research, 71-2 Jang-Dong, Yuseong-Gu, Daejeon 305-343, Republic of Korea

ARTICLE INFO

Article history:
Received 30 January 2009
Received in revised form 4 March 2009
Accepted 8 March 2009
Available online 20 March 2009

Keywords:
Ni_3Al foil
Ni catalysts
Spontaneous activation
Methanol decomposition
Steam addition

ABSTRACT

Methanol decomposition was carried out under steam addition (steam-to-carbon ratio (S/C) = 0–2.0) over cold-rolled Ni_3Al foils at temperatures ranging from 513 to 793 K. The spontaneous activation was clearly observed at S/C = 0.1 and below, while suppressed at S/C = 0.5 and above. Surface characterization of the spent foils revealed that fine Ni particles were formed at S/C = 0.1 and below due to the selective oxidation/hydroxylation of Al, while further steam addition suppressed it due to the oxidation/hydroxylation of both Al and Ni. The results confirm the spontaneous activation mechanism due to the formation of fine Ni particles which is induced by the selective oxidation/hydroxylation of Al. Reaction analysis revealed that methanol decomposition mainly occurred even under steam addition. It also revealed the effect of steam addition on the minor side reactions, methanation, water-gas shift reaction and carbon deposition.

1. Introduction

An efficient hydrogen production from alcohols or hydrocarbons is important in the development of fuel cell [1–5]. Micro-channeled reactors are highly promising for this purpose due to their high surface-to-volume ratio and high rates of heat and mass transfer compared with conventional reactors [6–9]. At present, it is a crucial issue for micro-channeled reactors to develop efficient and inexpensive heterogeneous catalysts. Another important issue is the development of heat-resistant metal sheets that can serve as support of catalyst layers and also structure sheets for the reactors.

The intermetallic compound Ni_3Al, the target material in this study, has considerable advantages in terms of its high-temperature mechanical properties [10,11]. Thus far, we have successfully fabricated thin foils of this compound by cold-rolling techniques [12,13] and demonstrated their capability of assembling honeycomb monolith and micro-channeled reactors [14]. Furthermore, we have recently found that the Ni_3Al foils show high catalytic activity for methanol decomposition into H_2 and CO in spite of their small surface area [15–17]. In the Ni–Al system there are four stable intermetallic compounds, $NiAl_3$, Ni_2Al_3, NiAl and Ni_3Al. Among them a mixture of $NiAl_3$ and Ni_2Al_3 is known as a precursor alloy of Raney nickel catalysts: Raney nickel catalysts are produced from the precursor alloy by alkali leaching. While methanol decomposition is accompanied by methanation and the water-gas shift reaction over Raney nickel catalysts [18] as well as Ni/SiO_2 [19], these side reactions are considerably suppressed over the Ni_3Al catalyst [15]. These results demonstrate the high potential of Ni_3Al foils as both structural sheets and catalysts for micro-channeled reactors used in the production of hydrogen.

Interestingly, the catalytic activity of the Ni_3Al foils was found to increase with the reaction time, indicating that the Ni_3Al foils spontaneously activate during methanol decomposition [15–17]. This unusual spontaneous activation of flat Ni_3Al foils can be attributed to the gradual formation of fine Ni particles on the foil surface during the reaction. The authors proposed that the fine Ni particles were produced through selective oxidation and/or hydroxylation of Al in Ni_3Al foils [15–17]. Selective Al oxidation and/or hydroxylation are considered to occur under very low oxidation and/or hydroxylation potential conditions. This special atmosphere likely occurs because only a small amount of H_2O is formed as a by-product during the reaction. These considerations suggest that steam plays a critical role in the spontaneous activation process. Thus, it is important to examine the effects of steam addition on the spontaneous activation in our newly discovered Ni_3Al foil catalysts during methanol decomposition.

* Corresponding author at: Department of Materials Science and Engineering, KAIST, 373-1, Guseong-dong, Yuseong-gu, Daejeon 305-701, Republic of Korea. Tel.: +82 42 350 4255; fax: +82 42 350 4275.
E-mail address: juni1394@kaist.ac.kr (J.H. Jang).

1381-1169/$ – see front matter © 2009 Elsevier B.V. All rights reserved.
doi:10.1016/j.molcata.2009.03.005

In the present study, methanol decomposition is carried out over cold-rolled thin Ni_3Al foils under various degrees of steam addition. The effects of steam addition on the spontaneous activation process and the catalytic reaction are discussed based on the results.

2. Experimental

Ni_3Al foils 30 μm in thickness were fabricated by the 98% cold-rolling of single crystalline plates of Ni_3Al (Ni–24 at.% Al) without intermediate annealing. Details of the foil fabrication procedure are available in literature [12,13]. Catalytic experiments were carried out over the foil samples in a conventional fixed-bed flow reactor at ambient pressure, in a process similar to that described previously [15–18,20,21]. Prior to the measurement, the samples were reduced at 513 K for 1 h in flowing hydrogen. After flushing the hydrogen with nitrogen, reactant mixtures with various steam-to-carbon ratios (S/Cs), S/C = 0, 0.1, 0.5, 1.0 and 2.0, were introduced to the reactor. The methanol injection rate was fixed at a constant liquid hourly space velocity (LHSV at STP) of 0.0011 $m^3\,h^{-1}\,m^{-2}$ (defined as the volume of methanol passed over the unit geometrical surface area of the foil sample per hour) and the water injection rate was changed to the desired S/Cs. All of the reactants were fully vaporized in a thermal evaporator at 433 K before being introduced to the reactor. The outlet composition was analyzed using two GCs equipped with thermal conductivity detectors (TCD) (GL Science, GC323). The total flow rate of the outlet gases excluding water and methanol was measured with a soap bubble meter. As the samples were in flat foil form, unlike common catalysts, the production rate of gases was calculated in mol $h^{-1}\,m^{-2}$ using the equation

$$R_i = \frac{C_i \times F_{\text{Total}}}{A} \quad (1)$$

where R_i is the production rate of gaseous species i, C_i is the volume fraction of gaseous species i in the total amount of outlet gases excluding the gasified CH_3OH and H_2O, F_{Total} is the flow rate of total amount of outlet gases (mol h^{-1}) excluding the gasified CH_3OH and H_2O, and A is the geometrical surface area of the foil sample.

The surface morphology of the samples after the reaction was observed by means of scanning electron microscopy (SEM) using a JEOL model JSM-7000F with a field emission gun. The BET (Brunauer–Emmett–Teller) surface areas of the samples were determined by krypton adsorption using a surface area analyzer (Micromeritics model ASAP2020). The surface area of each sample ($m^2\,m^{-2}$) was expressed as the measured BET surface area for the unit geometrical surface area of the foil samples. The amount of deposited carbon was analyzed by means of thermogravimetric analysis (TGA) using a Shimadzu model DTG-60H. The crystal structures of the surface products were characterized by X-ray diffraction (XRD) with Rigaku RINT 2500 V using a Cu Kα source. The electron binding energies (BE) of nickel, aluminum and oxygen in the Ni_3Al foils were measured by means of X-ray photoelectron spectroscopy

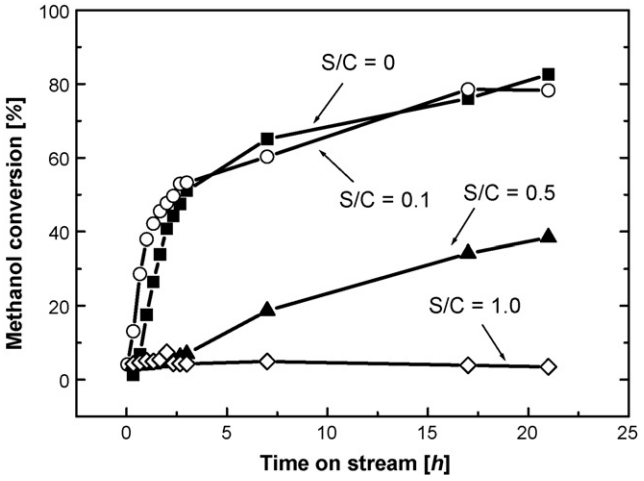

Fig. 2. Methanol conversion over Ni_3Al foils at 793 K as a function of the reaction time.

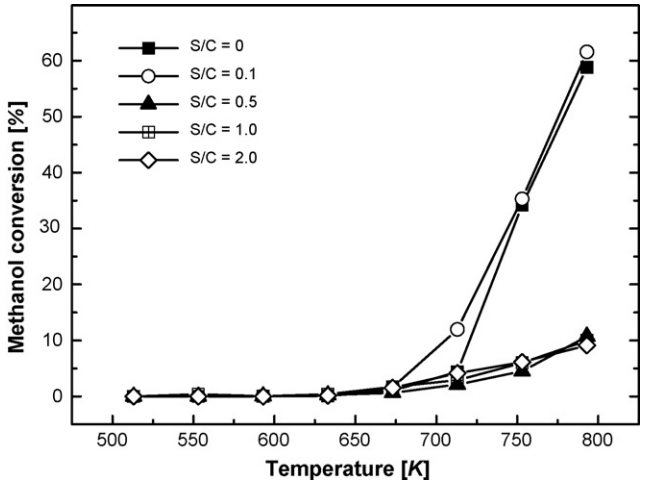

Fig. 1. Methanol conversion over Ni_3Al foils at various S/Cs as a function of the reaction temperature.

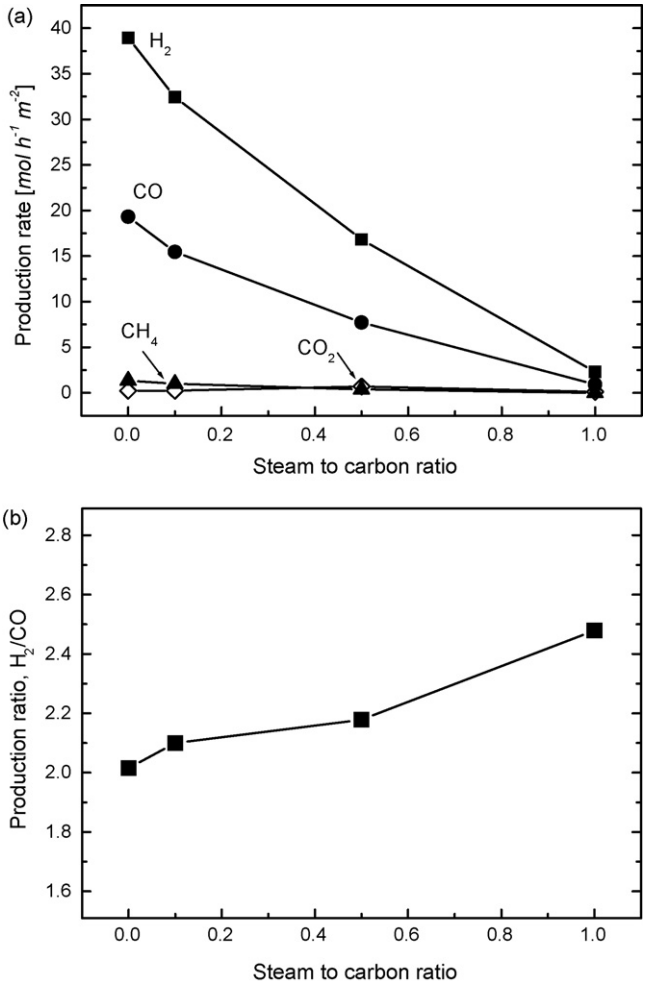

Fig. 3. Effects of steam addition on (a) the production rate of H_2, CO, CO_2 and CH_4 and (b) the production ratio of H_2 to CO after 21 h of reaction at 793 K.

(XPS) using a VG Scientific model ESCALab 200R with a twin anode Al Kα X-ray source (1486.6 eV; 250 W) and a hemispherical energy analyzer. The spectra were corrected by referring them to the Ni 3p spectrum (binding energy 66 eV) of metallic Ni obtained from pure Ni foils, in the same way as we previously reported [16]. The BE and full width at half maxima (FWHM) were kept constant for the same metallic component or oxide/hydroxide component throughout the fitting procedure.

3. Results

3.1. Catalytic properties

The catalytic performance of the cold-rolled Ni_3Al foils for methanol decomposition was surveyed under various S/Cs from 0 to 2.0 as the reaction temperature was increased stepwise from 513 to 793 K. Fig. 1 shows the methanol conversion as a function of the reaction temperature. The methanol conversion was very low below 713 K for all S/Cs, whereas it increased with the temperature above 713 K, indicating the onset of catalytic activation. Steam addition had a strong effect on the extent of the catalytic activation but little effect on the onset temperature. The catalytic activation was clearly observed at S/C = 0 and 0.1, though it became very low as the S/C exceeded 0.5.

The time dependence of the methanol conversion was examined at a constant temperature of 793 K, i.e., over the onset temperature. Fig. 2 shows the methanol conversion as a function of the reaction time. We carried out the reaction test two times under each condition to check the reproducibility. The difference in methanol conversion between the two tests was less than 9.2, 12.2, 19.6 and 3.2% throughout the test period at S/C = 0, 0.1, 0.5 and 1.0, respectively. At S/C = 0, the methanol conversion rapidly increased with the reaction time within the initial several hours and then reached a steady-state after 29 h. This result indicates that the cold-rolled Ni_3Al foils are spontaneously activated during the reaction test, as Chun et al. [15,16] reported . It is important to note that the spontaneous activation strongly depended on the S/C. At S/C = 0.1 the spontaneous activation occurred in a manner similar to the case of S/C = 0 but became lower as S/C increased and hardly occurred at S/C = 1.0. It is apparent that the steam addition suppressed the spontaneous activation of the Ni_3Al foils.

Fig. 3(a) plots the production rates of the gaseous products as a function of S/C after 21 h of reaction at 793 K, where the initial rapid activation had finished. Among these rates, the production rates of H_2 and CO were much higher at all S/Cs compared to those of other gaseous products. Clearly, methanol decomposition (Eq. (2)) occurred as the main reaction under all S/C conditions:

$$CH_3OH(g) \leftrightarrow CO(g) + 2H_2(g) \quad (2)$$

Both the production rates of H_2 and CO decreased as S/C increased, corresponding to the decrease in the methanol conversion (Fig. 2). The ratio of both production rates, H_2/CO, is plotted in Fig. 3(b). At S/C = 0, the ratio was nearly 2, showing a stoichiometric relationship for methanol decomposition into H_2 and CO (Eq. (2)). However, it increased to a value in excess of 2 as S/C increased, indicating that side reactions that produce H_2 and/or consume CO were induced by the steam addition. The production rates of minor gaseous products, CH_4 and CO_2, changed slightly as the S/C increased, though both values were very low for all S/Cs; the production rate of CH_4 decreased from 1.3 to 0 mol h^{-1} m^{-2} as S/C increased from 0 to 1.0. In addition, that of CO_2 slightly changed from 0.2 to 0.1 mol h^{-1} m^{-2}. Compared to Raney nickel catalysts [18], the production of CH_4 and CO_2 was suppressed under all S/C conditions.

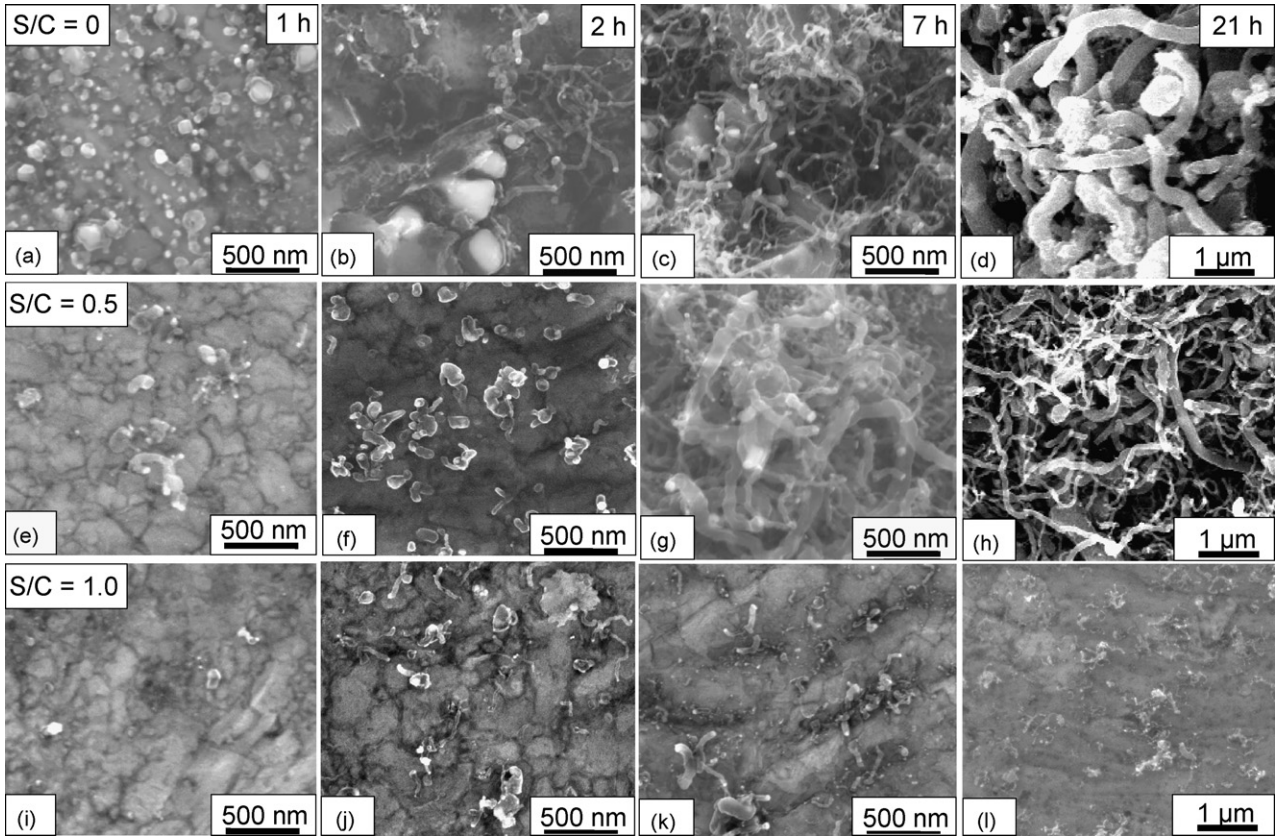

Fig. 4. Surface SEM images of Ni_3Al foils after (a, e, i) 1 h, (b, f, j) 2 h, (c, g, k) 7 h, and (d, h, l) 21 h of reaction at 793 K: (a–d) S/C = 0, (e–h) S/C = 0.5 and (i–l) S/C = 1.0.

3.2. Surface characterization

Surface observation by SEM, as shown in Fig. 4, revealed an evolution of solid phase products on the foil surface during the reaction at 793 K. Before the reaction, the surface was macroscopically smooth (not shown here) [16,17]. The surface evolution at S/C = 0 was previously identified by Chun et al. [15,16] using XRD and STEM–EDS; small Ni particles formed on the foil surface after 1 h of reaction (Fig. 4a), and carbon fibers subsequently grew from the surface of the Ni particles after 2 h of reaction (Fig. 4b). Thereafter, the density of both Ni particles and carbon fibers increased over the entire surface of the foils as the reaction time increased (Fig. 4c and d). In the present study, the size and distribution of the Ni particles were examined after 1 h of reaction (corresponding to Fig. 4a) using the back-scattered electron image in the SEM. Fig. 5a shows that the Ni particles (bright particles denoted by the arrows in the figure) were less than 250 nm in diameter and were uniformly distributed

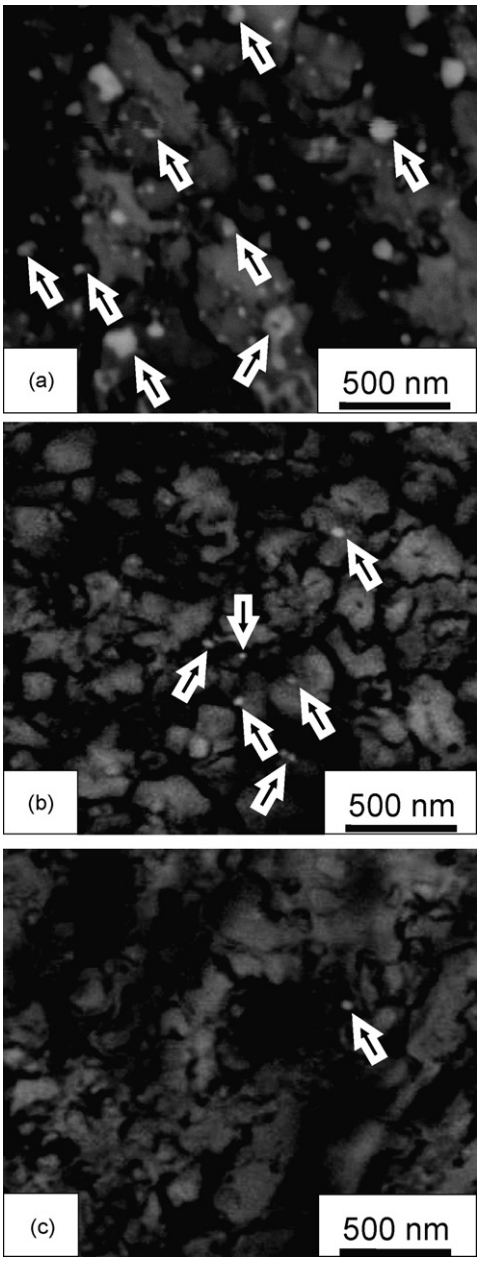

Fig. 5. Back-scattered electron images of Ni_3Al foils after 1 h of reaction at 793 K, showing Ni particles (arrows): (a) S/C = 0; (b) S/C = 0.5; (c) S/C = 1.0.

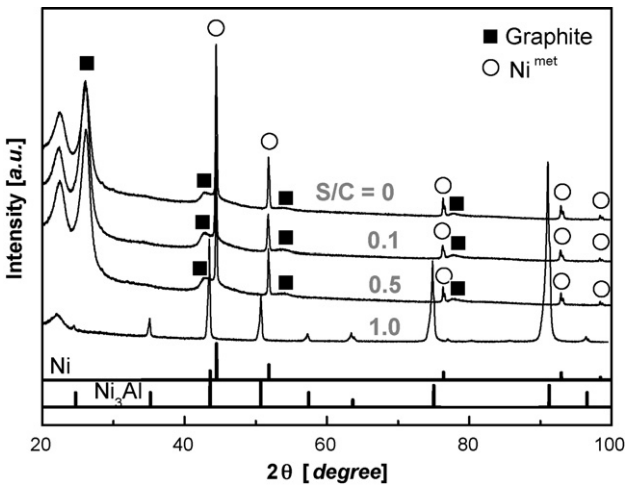

Fig. 6. XRD pattern for cold-rolled Ni_3Al foils after 21 h of reaction at 793 K.

on the surface. Nearly the same surface evolution was observed at S/C = 0.1 (data not shown here). At S/C = 0.5, Ni particles also formed after 1 h of reaction (Fig. 4e). They were, however, small in size and sparsely distributed compared with those at S/C = 0, as shown in the corresponding back-scattered electron image (Fig. 5b). Clearly, the steam addition retarded Ni particle formation. The formation of carbon fibers was also retarded compared to that at S/C = 0 (comparing Fig. 4b and f). At S/C = 1.0, the formation of both surface products was further retarded. The amount of produced Ni particles was extremely small after 1 h of reaction, as shown in the corresponding back-scattered electron image (Fig. 5c). Carbon fibers barely formed through entire range of reaction time (Fig. 4j–l). These results reveal a close relationship between the spontaneous activation and the formation of Ni particles accompanied with the formation of carbon fibers. This supports the spontaneous activation mechanism previously proposed by the authors, in which the produced Ni particles catalyze the two reactions of methanol decomposition and the formation of carbon fibers [15,16].

Fig. 6 shows the XRD pattern of the foil samples after 21 h of reaction at 793 K. The patterns show that metallic Ni and graphite formed on the foil surface under the condition of $S/C \leq 0.5$, whereas they did not appear at S/C = 1.0. This confirms that the steam addition suppressed the formation of the Ni particles and, as a result, the formation of carbon fibers. This is consistent with the SEM observation.

As shown in Fig. 4, carbon fiber grew from the surface of the Ni particles as a by-product. TG analysis was carried out to measure the amount of the deposited carbon fibers. Fig. 7 shows the TGA spectra of the foil samples after 21 h of reaction at 793 K. Weight loss was observed from 773 to 973 K for the samples reacted at $S/C \leq 0.5$, indicating that the carbon fibers burn in an air atmosphere [22,23]. The amount of the deposited carbon was evaluated from the weight loss, as summarized in the first row of Table 1. It increased as S/C increased in the range of $S/C \leq 0.1$ and then decreased in the range of $S/C \geq 0.5$. Very little carbon was precipitated at S/C = 1.0.

The BET surface areas of the Ni_3Al foils before and after 7 h of reaction at 793 K are given in Table 2. The surface area before the reaction was approximately 17 $m^2\,m^{-2}$, which indicates that the BET surface area of the cold-rolled Ni_3Al foils is roughly 17 times greater than the geometrical value. After 7 h of reaction at S/C = 0, the surface area increased significantly to nearly 890 $m^2\,m^{-2}$. This is approximately 50 times as large as the value before the reaction. The remarkable increase in the surface area is clearly due to the formation of the fine Ni particles and the carbon fibers on the foil surface, as shown in Fig. 4c. By comparison, the surface area did not

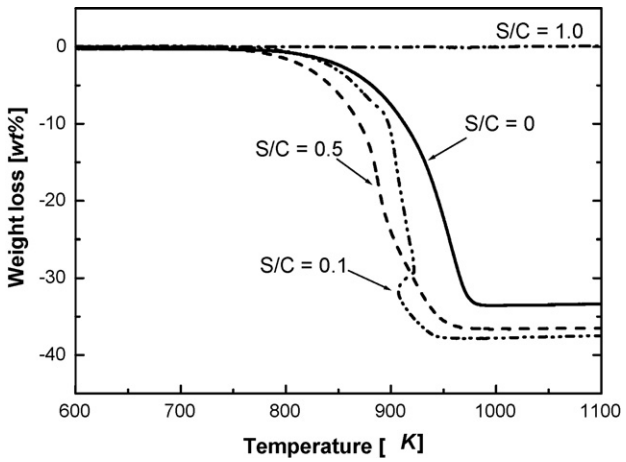

Fig. 7. TGA curves of Ni_3Al foils after 21 h of reaction at 793 K.

Table 1
Amount of deposited carbon (mol m^{-2}) after 21 h of reaction at 793 K.

Condition	Carbon deposition[a] [mol m^{-2}]	Conversion [%]	Converted methanol[b] [mol m^{-2}]	Carbon/methanol[c] [%]
S/C = 0	4.63	83	335	1.4
S/C = 0.1	5.57	78	304	1.8
S/C = 0.5	5.27	38	102	5.2
S/C = 1.0	0.01	4	25	<0.1

[a] Amount of carbon formation obtained by TGA measurement.
[b] Total amount of converted methanol during 21 h of reaction.
[c] Ratio of carbon deposition to total amount of converted methanol.

increase as much under the steam addition, which is reflected on the surface morphology (Fig. 4g and k). The values were close to 150 and 108 m^2 m^{-2} after 7 h of reaction at S/C = 0.5 and 1.0, respectively.

The surface chemical states of the foils in the initial period of reaction were analyzed using XPS. Fig. 8a shows the Al 2p/Ni 3p spectra after 1 h of reaction at S/C = 1.0 compared to those before and after 1 h of reaction at S/C = 0 as previously reported by Chun et al. [16]. Before the reaction, the Al 2p spectrum showed two peaks at 72.4 and 74.5 eV that correspond to the binding energies of metallic Al (Al^{met}) and amorphous Al oxide (AlO_X), respectively [15–17,24]. This indicates the existence of native oxide on the foil surface before the reaction [24]. After the reaction at S/C = 0, both the Al^{met} and AlO_X peaks disappeared and were replaced by a peak at 75.8 eV, indicating the formation of Al_2O_3 and/or $Al(OH)_3$. The O 1s spectrum (Fig. 8b) can be suitably fitted by two components at 532.7 and 533.9 eV, which correspond to the binding energies of Al_2O_3 and $Al(OH)_3$, respectively. In contrast, Ni remained metallic. Neither Ni oxide nor Ni hydroxide was detected in both the Ni 3p and O 1s spectra. Thus, the Al in Ni_3Al was selectively oxidized and hydroxylated to form Al_2O_3 and $Al(OH)_3$ at S/C = 0 [16]. In the case of the reaction at S/C = 1.0, the Al 2p spectrum showed characteristics that were nearly identical to those at S/C = 0, indicating the formation of Al_2O_3 and $Al(OH)_3$. However, the Ni 3p spectrum showed two additional peaks at 67.5 and 68 eV corresponding to the binding energies of NiO and $Ni(OH)_2$, respectively [25]. The O 1s spectrum was well fitted by the component of these Ni compounds [25,26] (Fig. 8b). The results clearly show that both Al and Ni in Ni_3Al were oxidized and hydroxylated to form Al_2O_3, $Al(OH)_3$ and $Ni(OH)_2$ and NiO. As the O 1s intensity for NiO was very low compared to that of other oxides and hydroxides, the amount of NiO was most likely small.

Table 2
BET surface area (m^2/m^2) of Ni_3Al foils before and after 7 h of reaction at 793 K. Measured BET surface areas (m^2) were normalized to the geometric surface area (m^2).

Before reaction [m^2 m^{-2}]	After 7 h of reaction [m^2 m^{-2}]		
	S/C = 0	S/C = 0.5	S/C = 1.0
16.6	887	150	108

Table 3
Partial pressures of H_2, CO, H_2O, CH_4 and CO_2 in the effluent after 1 h of reaction at 793 K over Ni_3Al foils.

S/C	Partial pressure [kPa]					Pressure ratio
	H_2	CO	H_2O	CH_4	CO_2	H_2/H_2O
0	17.9	9.0	2	0.1	<0.1	9.0
0.1	29.9	15.2	7	0.5	<0.1	4.3
0.5	3.6	1.7	21	–	<0.1	0.2
1.0	3.5	1.6	32	<0.1	<0.1	0.1

4. Discussion

4.1. Activation process

Steam addition significantly affected the spontaneous activation of the cold-rolled Ni_3Al foils, as shown in Fig. 2. Spontaneous activation favorably occurred at S/C = 0.1 and below but became lower as the S/C increased until it was only slightly observed at S/C = 1.0. Surface characterization of the spent samples revealed that excessive steam addition suppressed the formation of fine Ni particles on the foil surface (Fig. 5) considerably because the Ni in Ni_3Al was oxidized and hydroxylated with increased S/C (Fig. 8). These results suggest that the steam addition significantly increased the oxidation and hydroxylation potentials in the reaction atmosphere.

It is important to discuss thermodynamically the oxidation and hydroxylation behaviors of Ni_3Al at various S/Cs. Table 3 lists the measured partial pressures of H_2, CO, H_2O, CH_4 and CO_2 in the effluent after 1 h of reaction at 793 K over the Ni_3Al foils. This condition is that in which the surface chemical state of the foils was examined by XPS in Fig. 8. In this atmosphere, there are two possible cases for oxidation/hydroxylation and the reduction of metals, the first of CO–CO_2 and the second of H_2–H_2O systems. Regarding the case of the CO–CO_2 system, the atmosphere can be highly reducing because the partial pressure of CO_2 is extremely low. There is therefore no chance of the oxidation and hydroxylation of Ni and Al, which disagrees with the present results. By comparison, the partial pressure ratio of H_2 to H_2O exists in a reasonable range. The following oxidation can be assumed:

$$Ni(s) + H_2O(g) \leftrightarrow NiO(s) + H_2(g) \quad (3)$$

$$2Al(s) + 3H_2O(g) \leftrightarrow Al_2O_3(s) + 3H_2(g) \quad (4)$$

Hydroxylation/dehydroxylation of metals occurs only in the H_2–H_2O system. The following reaction can be assumed:

$$Ni(s) + 2H_2O(g) \leftrightarrow Ni(OH)_2(s) + H_2(g) \quad (5)$$

$$2Al(s) + 6H_2O(g) \leftrightarrow 2Al(OH)_3(s) + 3H_2(g) \quad (6)$$

Based on the above assumption, the equilibrium partial pressures of H_2 and H_2O for the reactions (3)–(6) can be calculated using Thermo-Calc, software for computational thermodynamics and the database SSUB3. The standard Gibbs free energy change at 793 K was obtained from Thermo-Calc and the equilibrium constant K_P was then calculated. These values are listed in Table 4. The equilibrium partial pressures of H_2 and H_2O were calculated from K_P and were plotted in a H_2–H_2O diagram, as shown in Fig. 9. The metal is in equilibrium with its oxide or hydroxide on the line and is stable compared to its oxide or hydroxide above the line, and vice versa. The measured partial pressures of H_2 and H_2O in Table 3

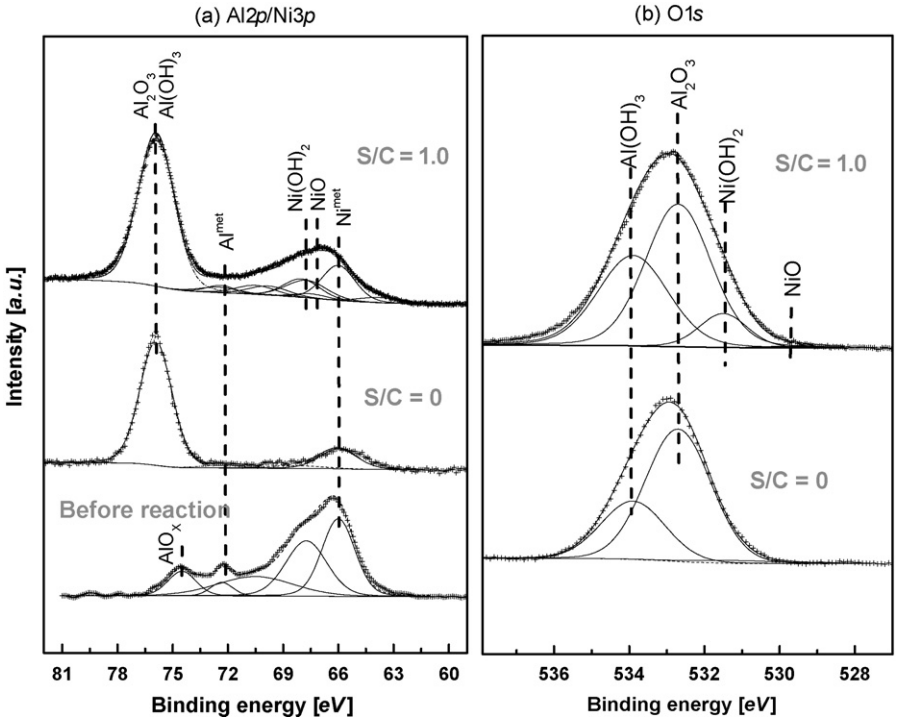

Fig. 8. XPS spectra obtained from cold-rolled Ni_3Al foils before and after 1 h of reaction at S/C = 0 and 1.0: (a) Al 2p/Ni 3p spectra for Ni_3Al foils before reaction, after 1 h of reaction at S/C = 0 and 1.0 (b) O 1s spectra for Ni_3Al foils after 1 h of reaction at S/C = 0 and 1.0.

Table 4
Standard Gibbs free energy change and equilibrium constant (K_P) for oxidation and hydroxylation of Al and Ni at 793 K.

Possible stoichiometric reactions	$\Delta G^{\circ}_{793\,K}$ [J/mol]	K_P
$2Al(s) + 3H_2O(g) \leftrightarrow Al_2O_3(s) + 3H_2(g)$	−815396	5.12×10^{53}
$2Al(s) + 6H_2O(g) \leftrightarrow 2Al(OH)_3(s) + 3H_2(g)$	−609793	1.47×10^{40}
$Ni(s) + H_2O(g) \leftrightarrow NiO(s) + H_2(g)$	36484	3.95×10^{-3}
$Ni(s) + 2H_2O(g) \leftrightarrow Ni(OH)_2(s) + H_2(g)$	100634	2.35×10^{-7}

are also plotted in Fig. 9. All of the plots were found to exist far below both the equilibrium state of Al_2O_3 and $Al(OH)_3$, predicting that both compounds are stable compared to metallic Al at all S/Cs. This is fairly consistent with the present experimental results: both Al_2O_3 and $Al(OH)_3$ were formed on the surface (Fig. 8). The diagram also predicts that metallic Ni is stable compared to NiO and $Ni(OH)_2$ under all S/C conditions. This state was observed at S/C = 0 and 0.1; metallic Ni particles were formed without the formation of NiO and $Ni(OH)_2$ (Figs. 5 and 8). It is thus thermodynamically understood that Al was selectively oxidized and hydroxylated and that Ni remained in a metallic state at S/C = 0.1 and below. However, the prediction in the results at S/C = 0.5 and 1.0 are inconsistent; NiO and $Ni(OH)_2$ coexisted with metallic Ni, which is in contrast to the prediction. This inconsistency suggests that in a case involving a high amount of steam addition, the foil surface is enriched in H_2O more than the overall gas composition. Hence, Ni can be partly oxidized and hydroxylated.

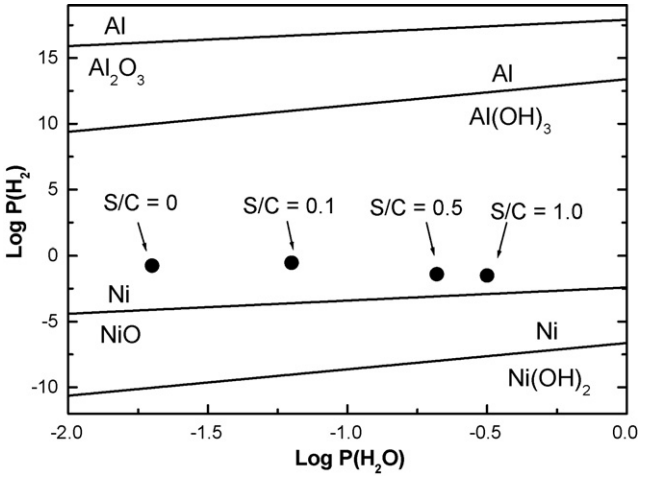

Fig. 9. Equilibrium partial pressure for oxidation/reduction and hydroxylation/dehydroxylation of Ni and Al in H_2–H_2O system at 793 K; the measured partial pressures of H_2 and H_2O in Table 3 are denoted by (●).

In a previous study, Chun et al. proposed a spontaneous activation mechanism due to the formation of fine Ni particles induced by selective oxidation and hydroxylation of Al [15–17]. First, Al in the Ni_3Al foils is selectively oxidized and hydroxylated to form Al_2O_3 and $Al(OH)_3$ during the initial period of reaction because of low oxidation and hydroxylation potentials in the reaction atmosphere with small amount of by-product H_2O. Ni atoms are left behind and aggregate into fine Ni particles on the foil surface. The produced Ni particles catalyze the main methanol decomposition, resulting in the production of H_2 and CO. They also catalyze the side reaction via the Boudouard reaction ($2CO \leftrightarrow C + CO_2$), resulting in the precipitation of carbon fibers on the Ni particles. The present study confirms the important role of the selective oxidation and hydroxylation of Al in the mechanism of Chun et al. from an opposite point of view. That is, if the selective oxidation and hydroxylation of Al is suppressed, e.g., by steam addition as in this study, only a minute number of fine Ni particles form and, eventually, the Ni_3Al foils are not spontaneously activated.

4.2. Reaction system

As shown in Fig. 3(a), the production rates of H_2 and CO were much higher compared to those of the other gas products in all S/C conditions. It became clear that steam addition lowered the

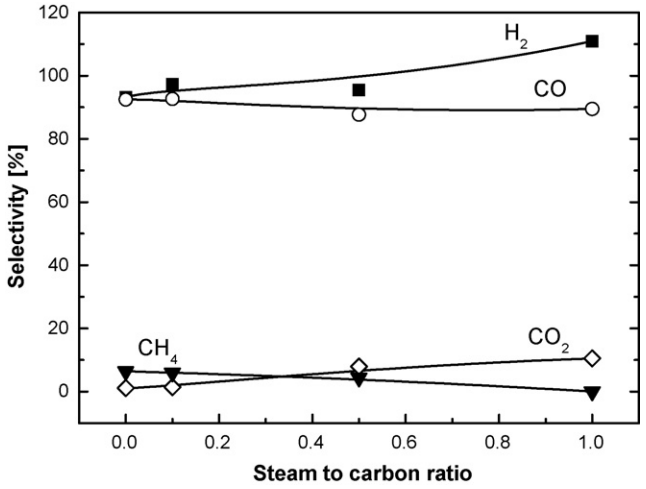

Fig. 10. Selectivity of H_2, CO, CH_4 and CO_2 after 21 h of reaction at 793 K over Ni_3Al foils.

methanol decomposition through the suppression of the Ni particle formation mechanism. However, as shown in Fig. 3(b), the ratio of both the production rates, (H_2/CO), deviated upward from the stoichiometric value of 2 for methanol decomposition as S/C increased, indicating that side reactions were enhanced as S/C increased. There was a small change in the production rates of the minor gaseous products CH_4 and CO_2. In addition, the amount of carbon fiber deposition varied depending on the characteristics of the steam addition (Table 1). The results show that the steam addition not only lowered the main methanol decomposition but also affected the minor side reactions to some extent. Thus, the effects of steam addition on the overall reaction system become important.

The selectivity of H_2 (S_{H_2}), and the other carbon-containing reaction products (S_x) can be calculated from the production rates of the products, as shown below.

$$S_{H_2} = \frac{R_{H_2}}{R_{CO} + R_{CH_4} + R_{CO_2}} \times \frac{1}{RR} \times 100 \quad (7)$$

$$S_x = \frac{R_x}{R_{CO} + R_{CH_4} + R_{CO_2}} \times 100 \quad (8)$$

here, R_{H_2}, R_{CO}, R_{CO_2} and R_{CH_4} are the experimentally measured production rates of H_2, CO, CO_2 and CH_4, respectively, and RR is the H_2/CO ratio in Eq. (2); the RR value for methanol decomposition is 2. Fig. 10 shows the calculated selectivities of various gaseous products after 21 h of reaction at 793 K. The selectivities of main gaseous products, H_2 and CO, showed very high values in excess of 90% under all S/C conditions compared to those of the by-products CH_4 and CO_2. Evidently, methanol decomposition (Eq. (2)) occurred as a main reaction even under steam addition conditions that were similar to the Ni and other VIII group metal catalyst cases [27–29]. Nevertheless, the selectivity of H_2 increased slightly as S/C increased, whereas that of CO remained mostly unchanged. This small change can be attributed to the side reactions, as discussed below.

The selectivities of the minor gaseous products were fairly small compared to those of the main products under all S/C conditions. The selectivity of CH_4 decreased from 6.4 to 0% as S/C increased from 0 to 1.0, whereas that of CO_2 increased from 1.1 to 10.5%. Chun et al. suggested that CH_4 and CO_2 are produced over Ni_3Al foils via the methanation of CO (Eq. (9)) and a water-gas shift reaction (Eq. (10)), respectively [15,16].

$$CO(g) + 3H_2(g) \leftrightarrow CH_4(g) + H_2O(g) \quad (9)$$

$$CO(g) + H_2O(g) \leftrightarrow CO_2(g) + H_2(g) \quad (10)$$

Steam addition will shift these reactions according to the principle of Le Chatelier, which implies that the methanation of CO (Eq. (9)) would be shifted to the reverse direction, leading to a decrease in the selectivity to CH_4, the water-gas shift reaction (Eq. (10)) in the forward direction, subsequently leading to an increase in the selectivity to CO_2. The present results are in good agreement with this principle, which confirms the validity of the suggestion of Chun et al.

The final side reaction, carbon deposition, varied with the steam addition (Table 1). Given that the methanol conversion also changed with the steam addition, the deposited carbon was normalized to the converted methanol, as shown in the fifth row of Table 1. The amount of deposited carbon increased as S/C increased up to S/C = 0.5, and significantly decreased above S/C = 0.5. Carbon deposition is considered through the Boudouard reaction [15]:

$$2CO(g) \leftrightarrow C(s) + CO_2(g) \quad (11)$$

This reaction is affected by steam addition through the water-gas shift reaction (Eq. (10)); consequently, the following reaction occurs [30,31]:

$$CO(g) + H_2(g) \leftrightarrow C(s) + H_2O(g) \quad (12)$$

Thus, steam addition will shift these reactions to the reverse direction: carbon deposition will be suppressed by steam addition. This trend was observed in the case of the steam addition above S/C = 0.5. However, the carbon deposition was enhanced by the small amount of steam addition below S/C = 0.5. The reason for this unexpected result is not well understood at present.

5. Conclusions

This study examined the effects of steam addition on the spontaneous activation in the cold-rolled Ni_3Al foil catalysts during methanol decomposition in the S/C range of 0–2.0 and in the temperature range of 513–793 K. The following results were obtained.

- Methanol mainly decomposed into H_2 and CO over the Ni_3Al foils even under steam addition. Spontaneous activation was observed in the initial stage of the decomposition.
- The spontaneous activation was clear and rapid at S/C = 0.1 and below, but became lower with further steam addition until it was scarcely observed at S/C = 1.0.
- Fine Ni particles were formed on the foil surface at the initial stage of reaction at S/C = 0.1 and below, while they became smaller in size and more sparse as S/C increased further, indicating that the spontaneous activation is due to the formation of the fine Ni particles.
- Al in the Ni_3Al foils was selectively oxidized and hydroxylated at S/C = 0.1 and below, while both Ni and Al were oxidized and hydroxylated at S/C = 1.0. These results support that the fine Ni particles are produced through the selective oxidation and hydroxylation of Al in Ni_3Al.
- It is considered that steam addition increases the oxidation and hydroxylation potentials in the reaction atmosphere, resulting in a change in the observed oxidation and hydroxylation behavior of Al and Ni.
- The results confirmed the spontaneous activation mechanism due to the formation of fine Ni particles which is induced by the selective oxidation/hydroxylation of Al.

Acknowledgements

This work was supported partly by the Korea Science and Engineering Foundation (KOSEF) grant funded by the Korean government (MOST) (No. R01-2007-000-10008-0), and a Grant-in Aid

for Scientific Research (KAKENHI) (C) (No. 19560774) and (B) (No. 19360321) from the Japan Society for the Promotion of Science.

References

[1] L.F. Brown, Int. J. Hydrogen Energy 26 (2001) 381–397.
[2] J.R. Rostrup-Nielson, Phys. Chem. Chem. Phys. 3 (2001) 283–288.
[3] J.M. Ogden, Phys. Today 55 (2002) 69–75.
[4] G.W. Crabtree, M.S. Dresselhaus, M.V. Buchanan, Phys. Today 57 (2004) 39–44.
[5] R. Vidil, C. Marvillet, Energy 30 (2005) 1233–1246.
[6] M.T. Janicke, H. Kestenbaum, U. Hagendorf, F. Schüth, M. Fichtner, K. Schubert, J. Catal. 191 (2000) 282–293.
[7] I. Aartun, H.J. Venvik, A. Holmen, P. Pfeifer, O. Görke, K. Schubert, Catal. Today 110 (2005) 98–107.
[8] X. Yu, S.T. Tu, Z. Wang, Y. Qi, Chem. Eng. J. 116 (2006) 123–132.
[9] Y. Kawamura, N. Ogura, T. Yamamoto, A. Igarashi, Chem. Eng. Sci. 61 (2006) 1092–1101.
[10] N.S. Stoloff, Int. Mater. Rev. 34 (1989) 153–183.
[11] N.S. Stoloff, C.T. Liu, S.C. Deevi, Intermetallics 8 (2000) 1313–1320.
[12] M. Demura, K. Kishida, Y. Suga, M. Takanashi, T. Hirano, Scr. Mater. 47 (2002) 267–272.
[13] M. Demura, Y. Suga, O. Umezawa, K. Kishida, E.P. George, T. Hirano, Intermetallics 9 (2001) 157–167.
[14] K. Kishida, M. Demura, S. Kobayasi, Y. Xu, T. Hirano, Defect Diffus. Forum 233–234 (2004) 37–48.
[15] D.H. Chun, Y. Xu, M. Demura, K. Kishida, D.M. Wee, T. Hirano, J. Catal. 243 (2006) 99–107.
[16] D.H. Chun, Y. Xu, M. Demura, K. Kishida, M.H. Oh, T. Hirano, D.M. Wee, Catal. Lett. 106 (2006) 71–75.
[17] D.H. Chun, Y. Xu, M. Demura, K. Kishida, M.C. Kim, M.H. Oh, T. Hirano, D.M. Wee, J. Korean Inst. Met. Mater. 43 (2005) 801–809.
[18] Y. Xu, S. Kameoka, K. Kishida, M. Demura, A.P. Tsai, T. Hirano, Intermetallics 13 (2005) 151–155.
[19] P.K. de Bokx, A.R. Balkende, J.W. Geus, J. Catal. 117 (1989) 467–484.
[20] Y. Xu, S. Kameoka, K. Kishida, M. Demura, A.P. Tsai, T. Hirano, Mater. Trans. 45 (2004) 3177–3179.
[21] Y. Ma, Y. Xu, M. Demura, D.H. Chun, G. Xie, T. Hirano, Catal. Lett. 112 (2006) 31–36.
[22] N.J. Welham, J.S. Williams, Carbon 36 (1998) 1309–1315.
[23] C.M. Chen, Y.M. Dai, J.G. Huang, J.M. Jehng, Carbon 44 (2006) 1808–1820.
[24] M. Haerig, S. Hofmann, Appl. Surf. Sci. 125 (1998) 99–114.
[25] N.S. McIntyre, M.G. Cook, Anal. Chem. 47 (1975) 2208–2213.
[26] A. Nylund, I. Olefjord, Surf. Interface Anal. 21 (1994) 283–289.
[27] Y. Matsumura, N. Tode, T. Yazawa, M. Haruta, J. Mol. Catal. A: Chem. 99 (1995) 183–185.
[28] N. Takezawa, N. Iwasa, Catal. Today 36 (1997) 45–56.
[29] J.S.J. Hargreaves, G. Ormsby, Catalysis 20 (2007) 107–121.
[30] F.W.A.H. Geurts, A. Sacco, Carbon 30 (1992) 415–418.
[31] P.E. Nolan, D.C. Lynch, A.H. Cutler, Carbon 32 (1994) 477–483.